Spectral Efficiency Analysis in Dense Massive MIMO Networks

FahimeSadat Mirhosseini*†, Andrea Pizzo†, Luca Sanguinetti†, Aliakbar Tadaion*

*Department of Electrical Engineering, Yazd University, Yazd, Iran

†Dipartimento di Ingegneria dell'Informazione, University of Pisa, Pisa, Italy

Abstract—This work considers the uplink of a Massive MIMO network wherein the base stations (BSs) are randomly deployed according to a homogenous Poisson point process of intensity λ. Each BS is equipped with M antennas and serves K user equipments. A rigorous stochastic geometry framework with a multi-slope path loss model and pilot-based channel estimation is used to analyze the impact of λ on channel estimation accuracy and spectral efficiency. Both maximum ratio and zero-forcing combiners are considered. Interesting analytical insights are provided into the interplay of network parameters such as λ, antenna-UE ratio M/K, and pilot reuse factor. The relative strength of pilot contamination and (inter- and intra-cell) interference is analytically and numerically evaluated, as a function of λ. It turns out that pilot contamination becomes relevant only for impractical values of $M/K \geq 100$.

I. INTRODUCTION

The data traffic in cellular networks has grown at an exponential pace for decades, thanks to the continuous evolution of the wireless technology. The traditional way to keep up with the traffic growth is to allocate more frequency spectrum. Consequently, there is little bandwidth left in the sub-6 GHz bands that are attractive for wide-area coverage. Another way is to reduce cell sizes by deploying more and more base stations (BSs) [1]. Quantitatively speaking, next generation of cellular networks foresees three different degrees of BS densification (on the basis of traffic load) [2]: low dense with roughly a BS density $\lambda \leq 10$ (measured in BS/km²), dense with $10 < \lambda < 100$ and ultra dense with $\lambda \geq 100$.

Typically, higher BS density leads to an irregular network deployment, which is well described by stochastic geometry tools [3]. These tools were used in [4] for single-input single-output (SISO) networks to show that the spectral efficiency (SE) is a monotonic non-decreasing function of λ. This result was proved by using a distance-independent path loss model. A more realistic model accounts for a multi-slope path loss, wherein the path loss exponent depends on the distance between user equipments (UEs) and BSs [5], [6]. With such a model, different operating regimes can be identified (as function of λ) for which an increase, saturation, or decrease of the SE is observed [7]. Despite this, multi-slope path loss models are not frequently used in cellular networks as they make the theoretical analysis much more demanding. An analytical simplification that still captures the essence of the model is discussed in [8], wherein the power decadence of the radiated signal is divided in two spatial half-spaces.

Nowadays, densification is not the only weapon in the hands of operators to increase the capacity of cellular networks. A very promising technology in this direction is Massive MIMO [9], [10], wherein BSs are equipped with a large number M of low-power, fully digital controlled, and physically small antennas to serve a multitude K of UEs by spatial multiplexing. A solid and mature theory for Massive MIMO has been developed in recent years, as underlined by the two recent textbooks [11], [12]. Remarkably, the long-standing pilot contamination issue, which was believed to impose a fundamental limitation [9], has recently been resolved in spatially correlated channels by using multicell processing [13], [14].

The aim of this work is to investigate the impact of BS densification on the uplink (UL) SE of Massive MIMO networks. The analysis is conducted on the basis of the theoretical framework developed in [6], which provides SE lower bounds in closed form by using a rigorous stochastic geometry-based framework and a general multi-slope path loss model. Analytical and numerical results are given for both maximum-ratio (MR) and zero-forcing (ZF) combining schemes by using the simplified dual-slope path loss model in [8]. This allows to gain several insights into the interplay among different network parameters, e.g., BS density, antenna-UE ratio M/K, and pilot reuse factor. Interesting observations are also made with respect to the impact and relative importance of (intra- and inter-) interference and pilot contamination in dense networks.

II. NETWORK MODEL

We consider the UL of a Massive MIMO cellular network wherein the BSs are spatially distributed at locations $\{\mathbf{x}_l\} \subset \mathbb{R}^2$ according to a homogenous Poisson point process $\Psi_\lambda = \{\mathbf{x}_l; l \in \mathbb{N}\}$ of intensity λ. Each BS has M antennas and serves simultaneously K single-antenna UEs. We use the nearest BS association rule so that the coverage area of a BS is its Poisson-Voronoi cell wherein the K UEs are uniformly distributed. The network operates according to the classical synchronous time-division-duplex protocol (TDD) over each coherence block [12], which is composed of τ_c complex-valued samples. In each coherence block, $\tau_p = K\zeta$ samples with ζ being the pilot reuse factor, are used for acquiring channel state information by means of UL pilot sequences.

A. Channel model

The channel $\mathbf{h}_{li}^j \in \mathbb{C}^M$ between the UE i in cell l and BS j is modeled as i.i.d. Rayleigh fading:

$$\mathbf{h}_{li}^j \sim \mathcal{N}_{\mathbb{C}}(\mathbf{0}_M, \beta_{li}^j \mathbf{I}_M) \tag{1}$$

where β_{li}^j is computed on the basis of a multi-slope path loss model [5]

$$\beta_{li}^j = \Upsilon_n (d_{li}^j)^{-\alpha_n} \tag{2}$$
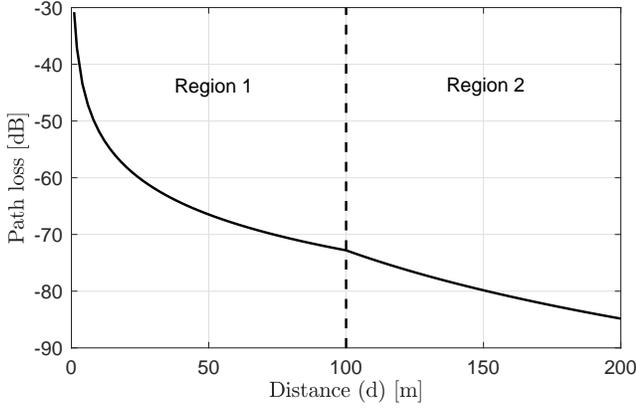
Fig. 1. Multi-slope path loss [dB] for the parameters listed in Table I.

TABLE I
TWO-SLOPE PATH LOSS MODEL.

R_n	Υ_n	α_n
$R_1 = 100$	$\Upsilon_1 = 8.3e - 04$, $\Upsilon_2 = 5.2481$	$\alpha_1 = 2.1$, $\alpha_2 = 4$

where $d_{li}^j \in [R_{n-1}, R_n)$, for $n = 1, \ldots, N$ denotes the distance of UE i in cell l from BS j, $0 \le \alpha_1 \le \cdots \le \alpha_N$ are the power decay factors, $0 = R_0 < \cdots < R_N = \infty$ denote the distances at which a change in the power decadence occurs, whereas $\Upsilon_{n+1} = \Upsilon_n R_n^{\alpha_{n+1} - \alpha_n}$ for $n = 1, \ldots, N-1$ are chosen for continuity purposes of the model with Υ_1 being a design parameter. Clearly, setting $N = 1$ yields the widely used single-slope path loss model, i.e., $\beta_{li}^j = \Upsilon_1 (d_{li}^j)^{-\alpha_1}$.

Although the subsequent analysis is valid for any path loss model, we follow [1], [5], [8] and use the dual-slope model, i.e., $N = 2$, illustrated in Fig. 1, with parameters reported in Table I. Particularly, we choose $R_1 = 100$ m[1] and assume $\alpha_1 = 2.1$ and $\alpha_2 = 4$. The coefficient Υ_2 ensures the continuity between the two regions. As discussed in [1], [5], [8], this model can be seen as a simplified version of the ITU-R UMi model [15].

B. Pilot allocation and power control

We assume that a pilot book $\{\boldsymbol{\Phi} \in \mathbb{C}^{\tau_p \times \tau_p}\}$ of τ_p orthonormal UL pilot sequences $\{\boldsymbol{\phi}_{li}\}_{i=1}^K$ is used for channel estimation in each cell $l \in \Psi_\lambda$. To avoid cumbersome pilot coordination as the network densifies, we assume that in each coherence block the BS l picks uniformly at random a subset of K different sequences from $\boldsymbol{\Phi}$ and distributes them among its served UEs [16]. Since $\tau_p = \zeta K$, we have that the reuse factor is $\zeta = \tau_p / K > 1$. In other words, there are on average $\mathbb{E}\{\Psi_\lambda\}/\zeta$ cells that share the same pilot subset. This is modeled in each cell through a Bernoulli stochastic variable $a_{l'l} \sim \mathcal{B}(1/\zeta)$ for $l' \neq l$ and $a_{ll} = 1$. Following [16], we assume that each UE uses a statistical channel inversion power-control policy such that

$$p_{li} = \rho / \beta_{li}^l \qquad (3)$$

[1]Typical values for ITU-R UMi model range from 20 to 200 m [1].
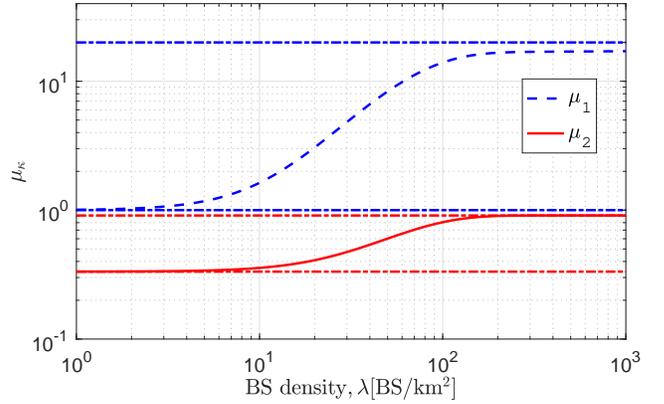
Fig. 2. Behavior of μ_1 and μ_2 as a function of λ [BS/km^2] for the path loss model in Table I.

where ρ is a design parameter. This ensures a uniform signal-to-noise ratio $\mathsf{SNR}_0 = \rho / \sigma^2$ across the network [16].

III. NETWORK ANALYSIS

The aim is to analyze the channel estimation accuracy and SE of the investigated Massive MIMO network as the BS density λ increases. The impact and relative importance of pilot contamination, induced by the so-called coherent interference [12], is also investigated. The analysis is conducted for the "typical UE", which is statistically representative for any other UE in the network [17]. Without loss of generality, we assume that the "typical UE" has an arbitrary index k and is connected to an arbitrary BS j.

A. Preliminaries

For later convenience, let us define the average coefficients μ_κ with $\kappa = 1, 2$ as in (4) where we use [6]

$$c_n(\kappa) = -\frac{R_n^{2-\kappa\alpha_n}}{\kappa\alpha_n - 2} \sum_{i=n+1}^N \left(\frac{\Upsilon_i}{\Upsilon_n}\right)^\kappa \frac{R_{i-1}^{2-\kappa\alpha_i} - R_i^{2-\kappa\alpha_i}}{\kappa\alpha_i - 2}. \qquad (5)$$

Both are needed for the analysis of channel estimation accuracy and SE. If a single-slope model with generic path loss coefficient α is adopted, μ_1 and μ_2 become

$$\mu_1 = \frac{2}{\alpha - 2} \qquad (6)$$

$$\mu_2 = \frac{1}{\alpha - 1} \qquad (7)$$

and are thus independent of the BS density λ. For the dual-slope model in Table I, the behavior of μ_1 and μ_2 as a function of λ is illustrated in Fig. 2. As seen, both coefficients are monotonic non-decreasing functions of λ and take values in the following intervals:

$$\frac{2}{\alpha_2 - 2} \le \mu_1 \le \frac{2}{\alpha_1 - 2} \qquad (8)$$

$$\frac{1}{\alpha_2 - 1} \le \mu_2 \le \frac{1}{\alpha_1 - 1} \qquad (9)$$

with μ_2 being much smaller than μ_1. Fig. 2 shows that the lower bounds are achieved for $\lambda \le 10$, which corresponds

$$\mu_\kappa = 2 \sum_{n=1}^{N} \frac{\Gamma\left(2; \pi\lambda R_{n-1}^2\right) - \Gamma\left(2; \pi\lambda R_n^2\right)}{\kappa\alpha_n - 2} + \frac{2c_n(\kappa)}{(\pi\lambda)^{\frac{\kappa\alpha_n}{2} - 1}} \left(\Gamma\left(1 + \frac{\kappa\alpha_n}{2}; \pi\lambda R_{n-1}^2\right) - \Gamma\left(1 + \frac{\kappa\alpha_n}{2}; \pi\lambda R_n^2\right)\right), \ \kappa = 1, 2 \quad (4)$$

to a low dense network wherein the probability for a UE to be in the second region of Fig. 1 is relatively high. The upper bounds are achieved for an ultra dense network with $\lambda \geq 10^2$. In this case, the UEs operate mostly in the first region. For $10 \leq \lambda \leq 10^2$, μ_1 and μ_2 increase monotonically and this basically accounts for scenarios that are a mixture of the two propagation conditions. Notice that the same trend is observed with a general N-slope path loss model. In this case, however, there are N ranges of values of λ wherein the coefficients μ_1 and μ_2 are equal to $\mu_1 = \frac{2}{\alpha_n - 2}$ and $\mu_2 = \frac{1}{\alpha_n - 1}$ for $n = 1, \ldots, N$.

B. Channel estimation

We call $\mathbf{Y}^j \in \mathbb{C}^{M \times \tau_p}$ the signal received at BS j during UL pilot transmission. The vector $\mathbf{y}_{jk}^j = \mathbf{Y}^j \boldsymbol{\phi}_{jk}^*$ takes the form:

$$\mathbf{y}_{jk}^j = \sqrt{\frac{\rho_{\mathrm{tr}}}{\beta_{jk}^j}} \mathbf{h}_{jk}^j + \sum_{l \in \Psi_\lambda \setminus \{j\}} a_{lj} \sqrt{\frac{\rho_{\mathrm{tr}}}{\beta_{li}^l}} \mathbf{h}_{lk}^j + \mathbf{n}_{jkj} \quad (10)$$

where $\mathbf{n}_{jkj}^{\mathrm{p}} \sim \mathcal{N}_{\mathbb{C}}(\mathbf{0}, \sigma^2 \mathbf{I}_M)$ and ρ_{tr} is a design parameter. The minimum mean-squared error (MMSE) estimate of $\mathbf{h}_{jk}^j$ based on $\mathbf{y}_{jk}^j$ is [12, Sec. 3.2]

$$\widehat{\mathbf{h}}_{jk}^j = \gamma_{jk}^j \frac{1}{\sqrt{\beta_{jk}^j \tau_p \rho_{\mathrm{tr}}}} \mathbf{y}_{jk}^j \sim \mathcal{N}_{\mathbb{C}}(\mathbf{0}, \gamma_{jk}^j \mathbf{I}_M) \quad (11)$$

with

$$\gamma_{jk}^j = \beta_{jk}^j \left(1 + \sum_{l \in \Psi_\lambda \setminus \{j\}} a_{lj} \frac{\beta_{lk}^j}{\beta_{lk}^l} + \frac{1}{\tau_p} \frac{1}{\mathsf{SNR}_0}\right)^{-1}. \quad (12)$$

The average NMSE is given by

$$\begin{aligned}
\mathsf{NMSE} &\triangleq \mathbb{E}_{\{\mathbf{d}, \mathbf{a}\}} \left\{ \frac{\mathbb{E}_{\{\mathbf{h}\}}\{\|\mathbf{h}_{jk}^j - \widehat{\mathbf{h}}_{jk}^j\|^2\}}{\mathbb{E}_{\{\mathbf{h}\}}\{\|\mathbf{h}_{jk}^j\|^2\}} \right\} \\
&= 1 - \mathbb{E}_{\{\mathbf{d}\}} \left\{ \frac{1}{\beta_{jk}^j} \mathbb{E}_{\{\mathbf{a}\}} \left\{ \gamma_{jk}^j \right\} \right\} \quad (13)
\end{aligned}$$

as it follows by taking the expectation with respect to the channel distributions. The following result is thus obtained.

Corollary 1 (Average NMSE). *The average NMSE can be upper bounded as:*

$$\mathsf{NMSE} \leq \overline{\mathsf{NMSE}} = 1 - 1/A(\mu_1) \quad (14)$$

with

$$A(\mu_1) = 1 + \frac{\mu_1}{\zeta} + \frac{1}{\zeta K} \frac{1}{\mathsf{SNR}_0}. \quad (15)$$

Proof: The proof follows from [6, Appendix A]. ∎

Corollary 1 shows that on average the NMSE is affected by pilot-sharing UEs through μ_1/ζ. Therefore, it reduces as
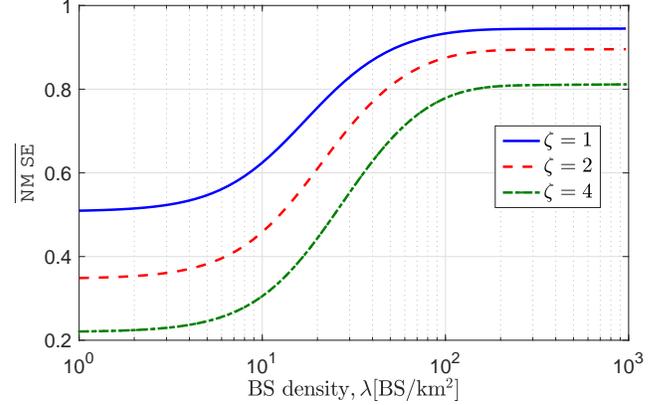
Fig. 3. $\overline{\mathsf{NMSE}}$ as a function of λ [BS/km^2] for the path loss model in Table I for $\zeta = \{1, 2, 4\}$ and $\mathsf{SNR}_0 = 5$ dB.

the pilot reuse factor ζ decreases and/or the BS density λ increases, which is due to the monotonicity of μ_1 with respect to λ. This is exemplified in Fig. 3 where $\overline{\mathsf{NMSE}}$ is plotted as a function λ for $\zeta \in \{1, 2, 4\}$ and $\mathsf{SNR}_0 = 5$ dB. As seen, $\overline{\mathsf{NMSE}}$ is lower and upper bounded and takes values in the interval:

$$1 - \frac{1}{A\left(\frac{2}{\alpha_2 - 2}\right)} \leq \overline{\mathsf{NMSE}} \leq 1 - \frac{1}{A\left(\frac{2}{\alpha_1 - 2}\right)} \quad (18)$$

where $A\left(\frac{2}{\alpha_2 - 2}\right)$ and $A\left(\frac{2}{\alpha_1 - 2}\right)$ are obtained after substituting the limits of μ_1 given by (8) into (15). The $\overline{\mathsf{NMSE}}$ is less than 0.6 for any ζ when $\lambda \leq 10$, i.e., a low dense network, but it increases fast as λ grows. In an ultra dense regime with $\lambda \geq 10^2$, e.g., it is higher than 0.8. Particularly, it approaches 0.95 with $\zeta = 1$. As shown later, this will have a strong negative impact on the SE. We notice also that increasing ζ brings less benefits (in terms of estimation accuracy) as λ becomes large. This is because the cell size decreases with λ and thus reducing the interference of pilot-sharing UEs by increasing their average distance has little impact as the network becomes denser and denser. Interestingly, $\overline{\mathsf{NMSE}}$ is very sensitive to densification in the interval $10 \leq \lambda \leq 10^2$. This implies that any additional BS in this regime comes with a higher cost (in terms of channel estimation accuracy) with respect to both cases $\lambda \leq 10$ and $\lambda \geq 10^2$.

C. Spectral Efficiency

We denote by $\mathbf{v}_{jk} \in \mathbb{C}^M$ the receive combining vector associated with UE k in cell j. Two popular choices for $\mathbf{v}_{jk}$ are MR and ZF [11]:

$$\mathbf{V}_j \triangleq [\mathbf{v}_{j1} \ \ldots \ \mathbf{v}_{jK}] = \begin{cases} \widehat{\mathbf{H}}_j^j & \text{with MR} \\ \widehat{\mathbf{H}}_j^j \left((\widehat{\mathbf{H}}_j^j)^{\mathsf{H}} \widehat{\mathbf{H}}_j^j\right)^{-1} & \text{with ZF} \end{cases} \quad (19)$$

$$\gamma^{\mathrm{MR}} = \cfrac{1}{\underbrace{\cfrac{A(\mu_1)}{M\mathsf{SNR}_0}}_{\text{Noise}} + \underbrace{\cfrac{K}{M}A(\mu_1)}_{\text{Intra-cell Interference}} + \underbrace{\cfrac{K}{M}\left(A(\mu_1)\mu_1 + \cfrac{\mu_2}{\zeta}\right)}_{\text{Inter-cell Interference}} + \underbrace{\cfrac{\mu_2}{\zeta}}_{\text{Pilot Contamination}}} \tag{16}$$

$$\gamma^{\mathrm{ZF}} = \cfrac{1}{\underbrace{\cfrac{A(\mu_1)}{(M-K)\mathsf{SNR}_0}}_{\text{Noise}} + \underbrace{\cfrac{K}{M-K}(A(\mu_1)-1)}_{\text{Intra-cell Interference}} + \underbrace{\cfrac{K}{M-K}A(\mu_1)\mu_1}_{\text{Inter-cell Interference}} + \underbrace{\cfrac{\mu_2}{\zeta}}_{\text{Pilot Contamination}}} \tag{17}$$

with $\widehat{\mathbf{H}}_j^j = [\widehat{\mathbf{h}}_{j1}^j \dots \widehat{\mathbf{h}}_{jK}^j] \in \mathbb{C}^{M \times K}$ containing the estimates of intra-cell channels in cell j. In a multicell Massive MIMO network with imperfect knowledge of the channel, they are both suboptimal [12], but widely applied in the literature because of their analytical tractability through the use-and-then-forget (UatF) bound for SE [11]. For the investigated network, the following result is obtained.

Lemma 1 (Average ergodic SE [6])**.** *If MMSE channel estimates are used and the UL powers are chosen as in (3), a lower bound on the UL average ergodic channel capacity is:*

$$\underline{\mathsf{SE}} = \left(1 - \frac{K\zeta}{\tau_c}\right)\log_2(1+\gamma) \tag{20}$$

where γ is given by (16) and (17) for MR and ZF, respectively.

One can make interesting observations from Lemma 1. With both schemes, the interference is decomposed into intra-cell and inter-cell interference. The first one accounts for the interference generated by the UEs located in the Poisson-Voronoi region of the serving BS, while the second one is due to all the other UEs. As seen, both terms reduce linearly with M if MR is used while they reduce with $M - K$ when ZF is employed.[2] This is because ZF sacrifices K spatial dimensions to suppress intra-cell interference. The same happens for the noise contribution. Moreover, we notice that both noise and (intra- and inter-) interference depend also on $A(\mu_1)$, which is due to the imperfect knowledge of the channel; see Corollary 1. Since $A(\mu_1)$ increases linearly with μ_1, both noise and interference grow as λ increases. The inter-cell interference term increases at an even faster rate with λ since it is a function of $A(\mu_1)\mu_1$. The last term μ_2/ζ in (16) and (17) accounts for pilot contamination since it is independent of the antenna-UE ratio M/K [12]. Interestingly, it is the same for both schemes. The following corollary is easily obtained.

Corollary 2. *When $M \to \infty$, $\gamma^{\mathrm{ZF}} = \gamma^{\mathrm{MR}} \asymp \gamma_{M \to \infty}$ with $\gamma_{M \to \infty} = \zeta/\mu_2$ and the ultimately achievable rate is*

$$R_{M \to \infty} = \left(1 - \frac{\zeta K}{\tau_c}\right)\log_2\left(1 + \frac{\zeta}{\mu_2}\right). \tag{21}$$

As shown in Fig. 2, μ_2 is much smaller than μ_1 for any λ. This implies that interference in (16) and (17) is likely the

---

[2]This is why the sum of the two is generally referred to as non-coherent interference [12].
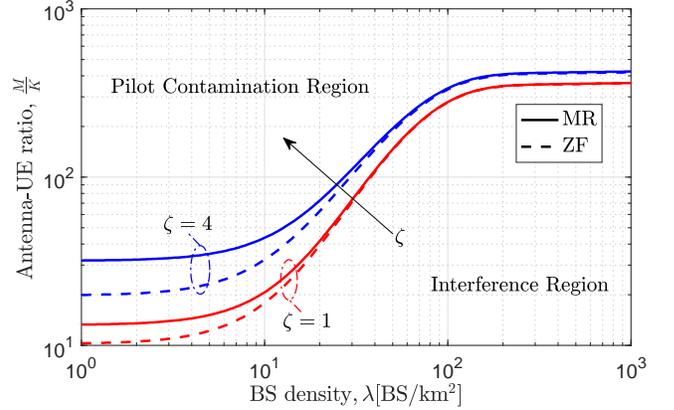
Fig. 4. Antenna-UE ratio M/K needed for the interference to equal pilot contamination as a function of λ. The dual-slope path loss model in Table I is adopted. Also, $\zeta = \{1, 4\}$ and $K = 10$.

dominating term of γ. To provide evidence of this, Fig. 4 illustrates the antenna-UE ratio M/K for which the interference and pilot contamination in (16) and (17) are equal to each other. The curves are plotted as a function of λ for $\zeta \in \{1, 4\}$ and must be understood in the sense that in the region above each one pilot contamination is higher than interference. As expected, for any λ the pilot contamination region with MR is smaller than that with ZF. This is because unlike MR, ZF mitigates the effect of intra-cell interference. The gap decreases as λ increases since inter-cell interference becomes more relevant. Remarkably, we observe that for practical values of M/K in the range interval $4 \leq M/K \leq 10$ [12], we never fall into the pilot contamination region regardless of λ and ζ. If large values are considered, i.e., $10 \leq M/K \leq 100$, interference always dominates pilot contamination for $\lambda \geq 50$. More generally, the results of Fig. 4 show that in dense and ultra-dense Massive MIMO networks interference is the major impairment. Pilot contamination becomes relevant only for impractical values of M/K.

To quantify the UL SE, Fig. 5 plots the lower bound in (20) versus λ with MR and ZF. Both schemes use the optimal pilot reuse factor, obtained by exhaustive search. We consider the practical value $M/K = 10$ but also $M/K = 50$. This latter case is used to evaluate the gap with the ultimately achievable rate in (21), which is also reported in Fig. 5. The asymptotically optimal pilot reuse factor is computed from Corollary 2 as follows.

Corollary 3. *When $M \to \infty$, the optimal pilot reuse factor ζ*
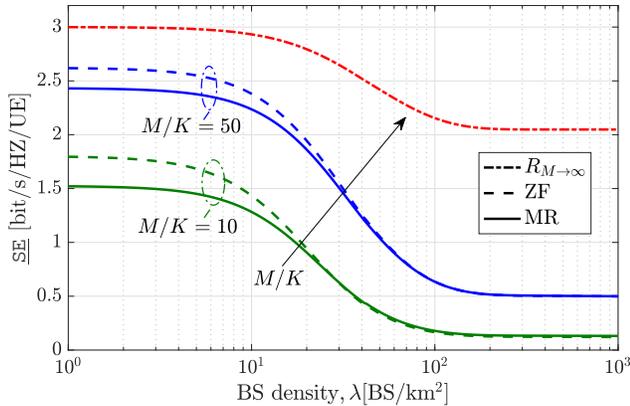
Fig. 5. $\underline{\text{SE}}$ as a function of λ [BS/km^2] for the dual-slope path loss model in Table I with $M/K = \{10, 50\}$, $K = 10$ and $\text{SNR}_0 = 5$ dB.

that maximizes (21) *is*

$$\zeta_{M\to\infty}^{\text{opt}} = \mu_2 \left(\frac{\nu}{W(\nu e)} - 1 \right) \tag{22}$$

where $W(.)$ is Lambert function and $\nu = 1 + \tau_c/(\mu_2 K)$.

Proof: By taking the derivative of (21) yields

$$\frac{\partial R_{M\to\infty}}{\partial \zeta} = -\frac{K}{\tau_c} \log_2 \left(1 + \frac{\zeta}{\mu_2} \right) + \frac{1 - \zeta K/\tau_c}{\mu_2 \ln(2)(1 + \zeta/\mu_2)}. \tag{23}$$

Setting $x = \frac{\tau_c/K - \zeta}{\mu_2 + \zeta}$ we obtain $(x+1)e^{x+1} = e(\frac{\tau_c}{K\mu_2} + 1)$, whose solution is easily found as $x = W(e(\frac{\tau_c}{K\mu_2} + 1)) - 1$. ∎

From Fig. 5, it is seen that $\underline{\text{SE}}$ is a monotonic non-increasing function of λ. This is because both interference and pilot contamination increase with λ through μ_1 and μ_2. Although ZF outperforms MR for $\lambda \leq 10$, the gain reduces as λ increases. Both schemes achieve the same performance for $\lambda > 30$. This is because inter-cell interference becomes the dominating term in (16) and (17) when the BSs are much closer to each other. We also notice that the gap with the ultimate achievable rate is substantial and increases with λ. Particularly, in an ultra dense network with $\lambda = 50$, MR and ZF achieve roughly 15% of $R_{M\to\infty}$ with $M/K = 10$. In the extreme case of $M/K = 50$, the gap is still large, though 45% of $R_{M\to\infty}$ is achieved.

Finally, we observe that the SE per UE maintains approximately constant in low dense, i.e., $\lambda \leq 10$, and ultra dense, i.e., $\lambda \geq 10^2$, networks. However, the area SE in bit/s/Hz/km^2 given by

$$\underline{\text{ASE}} = \lambda K \underline{\text{SE}} \tag{24}$$

increases linearly with λ in these regions. This implies that there are operating regimes in which we can linearly increase the ASE while keeping the same SE per UE across the network. While for $10 < \lambda < 10^2$, ASE will suffer from a small decrease.

IV. CONCLUSIONS

We studied the impact of BS densification on channel estimation and SE in the UL of Massive MIMO. The analysis

was conducted for MR and ZF with a two-slope path loss model. Lower bounds of the NMSE and SE were provided in closed forms from which interesting insights were obtained. Particularly, we quantified the relative importance of pilot contamination and (intra- and inter-) interference, and showed that the latter largely dominates for any BS density λ irrespective of the antenna-UE ratio M/K. We showed that the SE is a monotonic non-increasing function of λ, and also demonstrated that both MR and ZF provide low SE already for $\lambda \geq 10$ [BS/km^2], even when M/K takes large values (up to 50). This means that multicell signal processing (e.g., [13], [14]) is required if a dense Massive MIMO network needs to be deployed.

REFERENCES

[1] J. G. Andrews, X. Zhang, G. D. Durgin, and A. K. Gupta, "Are we approaching the fundamental limits of wireless network densification?" *IEEE Communications Magazine*, vol. 54, no. 10, pp. 184–190, October 2016.

[2] X. Ge, S. Tu, G. Mao, C.-X. Wang, and T. Han, "5G ultra-dense cellular networks," *IEEE Wireless Communications*, vol. 23, no. 1, pp. 72–79, 2016.

[3] J. G. Andrews, S. Buzzi, W. Choi, S. V. Hanly, A. Lozano, A. C. K. Soong, and J. C. Zhang, "What will 5G be?" *IEEE J. Sel. Areas Commun.*, vol. 32, no. 6, pp. 1065–1082, 2014.

[4] J. G. Andrews, F. Baccelli, and R. K. Ganti, "A tractable approach to coverage and rate in cellular networks," *IEEE Transactions on Communications*, vol. 59, no. 11, pp. 3122–3134, 2011.

[5] X. Zhang and J. G. Andrews, "Downlink cellular network analysis with multi-slope path loss models." *IEEE Trans. Communications*, vol. 63, no. 5, pp. 1881–1894, 2015.

[6] A. Pizzo, D. Verenzuela, L. Sanguinetti, and E. Björnson, "Network deployment for maximal energy efficiency in uplink with multislope path loss," *IEEE Transactions on Green Communications and Networking*, 2018.

[7] M. Ding and D. López-Pérez, "Performance impact of base station antenna heights in dense cellular networks," *IEEE Transactions on Wireless Communications*, vol. 16, no. 12, pp. 8147–8161, 2017.

[8] J. Arnau, I. Atzeni, and M. Kountouris, "Impact of los/nlos propagation and path loss in ultra-dense cellular networks," in *2016 IEEE International Conference on Communications (ICC)*, May 2016, pp. 1–6.

[9] T. L. Marzetta, "Noncooperative cellular wireless with unlimited numbers of base station antennas," *IEEE Transactions on Wireless Communications*, vol. 9, no. 11, pp. 3590–3600, 2010.

[10] E. G. Larsson, F. Tufvesson, O. Edfors, and T. L. Marzetta, "Massive MIMO for next generation wireless systems," *IEEE Commun. Magazine*, vol. 52, no. 2, pp. 186–195, Feb. 2014.

[11] T. L. Marzetta, E. G. Larsson, H. Yang, and H. Q. Ngo, *Fundamentals of Massive MIMO*. Cambridge University Press, 2016.

[12] E. Björnson, J. Hoydis, and L. Sanguinetti, "Massive MIMO networks: Spectral, energy, and hardware efficiency," *Foundations and Trends® in Signal Processing*, vol. 11, no. 3-4, pp. 154–655, 2017.

[13] E. Björnson, J. Hoydis, and L. Sanguinetti, "Massive MIMO has unlimited capacity," *IEEE Transactions on Wireless Communications*, vol. 17, no. 1, pp. 574–590, 2018.

[14] L. Sanguinetti, E. Björnson, and J. Hoydis, "Towards Massive MIMO 2.0: Understanding spatial correlation, interference suppression, and pilot contamination," *CoRR*, vol. abs/1904.03406, 2019.

[15] 3GPP, "Technical specification group radio access network; evolved universal terrestrial radio access (e-utra); further advancements for e-utra physical layer aspects (release 9). tr 36.814," Tech. Rep., 2010.

[16] E. Björnson, L. Sanguinetti, and M. Kountouris, "Deploying dense networks for maximal energy efficiency: Small cells meet massive mimo," *IEEE Journal on Selected Areas in Communications*, vol. 34, no. 4, pp. 832–847, 2016.

[17] F. Baccelli and B. Blaszczyszyn, "Stochastic geometry and wireless networks: Volume I Theory," *Foundations and Trends in Networking*, vol. 3, no. 3-4, pp. 249–449, 2008.